Journal of Power Sources 206 (2012) 259–266

Contents lists available at SciVerse ScienceDirect

Journal of Power Sources

journal homepage: www.elsevier.com/locate/jpowsour

$LiFePO_4$–Fe_2P–C composite cathode: An environmentally friendly promising electrode material for lithium-ion battery

Md. Mokhlesur Rahman[a,c,*], Jia-Zhao Wang[a], Rong Zeng[a], David Wexler[b], Hua Kun Liu[a]

[a] Institute for Superconducting and Electronic Materials & ARC Centre of Excellence for Electromaterials Science, University of Wollongong, NSW 2522, Australia
[b] School of Mechanical, Mechatronic & Materials Engineering, University of Wollongong, NSW 2522, Australia
[c] Institute for Technology Research and Innovation, Deakin University, Waurn Ponds, VIC 3217, Australia

ARTICLE INFO

Article history:
Received 1 December 2011
Received in revised form 10 January 2012
Accepted 12 January 2012
Available online 25 January 2012

Keywords:
Manual grinding
$LiFePO_4$–Fe_2P–C composite
Fe_2P phase
$LiFePO_4$/Fe_2P interface coupling
Li-ion batteries

ABSTRACT

In this investigation, the synthesis strategy is involved the creation of $LiFePO_4$–Fe_2P–C composites with a porous conductive architecture, which includes distinct regions or clusters containing antiferromagnetic $LiFePO_4$ in close proximity to ferromagnetic Fe_2P. The microstructure is achieved by using a simple ultra-fast solvent assisted manual grinding method, combined with solid state reaction, which can replace the time-consuming high energy ball milling method. The crystalline structure, morphology, and electrochemical characterization of the synthesised product are investigated systematically. The electrochemical performance is outstanding, especially the high C rate. The composite cathode is found to display specific capacity of 167 mAh g^{-1} at 0.2 C and 146 mAh g^{-1} at 5 C after 100 cycles, respectively. At the high current density of 1700 mA g^{-1} (10 C rate), it exhibits long-term cycling stability, retaining around 96% (131 mAh g^{-1}) of its original discharge capacity beyond 1000 cycles, which can meet the requirements of a lithium-ion battery for large-scale power applications. The obtained results have demonstrated that the fabrication of samples with strong and extensive antiferromagnetic and ferromagnetic interface coupling of $LiFePO_4$/Fe_2P provides a versatile strategy toward improving the electrochemical properties of $LiFePO_4$ materials and also opens up a new window for material scientists to further study the new exchange bias phenomenon and its ability to enhance the electrochemical performance of lithium-ion battery electrode.

1. Introduction

In this new century, clean and renewable energy storage devices have become important subjects for research and development in the energy, electronics, and transportation industries [1]. The urgency for renewal energy requires the use of clean energy sources at a much higher level than that presently in force. The CO_2 issue, and the consequent air pollution in large urban areas, may be only solved by replacing internal combustion engine (ICE) cars with ideally, zero emission vehicles, i.e. electric vehicles (EVs) or, at least, by controlled emission vehicles, i.e. hybrid electric vehicles (HEVs) and/or plug-in electric vehicles (PHEVs) [2,3]. Lithium ion batteries are considered close to becoming state-of-the-art technology for a range of advanced electrochemical energy storage and conversion systems. Thus, achieving the goals of low cost combined with higher energy density, better cycling stability, and non- or less toxic and more environmentally friendly materials as electrodes for lithium ion batteries has become mandatory if clean renewable technologies are to be developed for the future [1,4]. For a range of EV/HEV applications, however, commercial lithium-ion batteries cannot yet achieve the required combination of high energy density, high power, and high rate capability. Apart from the search for new or improved electrode materials with higher energy densities [5–7], the enhancement of electrode capacity retention at high charge/discharge rates is one of the main challenges in lithium-ion battery research. Following the pioneering work by Padhi et al. [8] olivine-like $LiFePO_4$ has become known as an attractive electrode material for lithium-ion batteries, for high power applications in particular. This is because of its high theoretical capacity (170 mAh g^{-1}), acceptable operating voltage (3.4 V vs. Li^+/Li), low cost, environmental friendliness, long cycle life, cell safety, and high thermal stability [2,8,9]. Nevertheless, a major limitation of this material, which prevents it from being used in large-scale applications, is its poor high-rate performance, owing to its low electronic conductivity and low ionic diffusion coefficient [10,11]. Furthermore, the long term cycling stability at high current rate is still a great challenge for this material, as it is a compulsory requirement for lithium ion batteries to have long cycle life for EV/HEV applications. Recently, ultra-fast charging and discharging at very high rates has been reported for $LiFePO_4$ material via creation of an ion conducting lithium phosphate coating on the surface

* Corresponding author. Tel.: +61 3 52272642, fax: +61 3 52271103.
E-mail addresses: mmr543@uowmail.edu.au, m.rahman@deakin.edu.au (Md.M. Rahman).

0378-7753/$ – see front matter © 2012 Elsevier B.V. All rights reserved.
doi:10.1016/j.jpowsour.2012.01.119

of $LiFePO_4$ nanoparticles, however, the reported cycle number is still not good enough [12]. Satisfactory long term cycling stability has been achieved through the formation of mesoporous $LiFePO_4$/C nanocomposite (118 mAh g^{-1} at 10 C after 1000 cycles) [2] and by synthesising $LiFePO_4$/carbon composite (~85 mAh g^{-1} at 10 C after 2400 cycles) via high-energy ball milling combined with a spray-drying method [13]. Both of these reported results satisfy the long term cycling requirements, but their specific discharge capacities are not as high as expect, and there is much more room for further improvement. In this investigation, the synthesis strategy has involved the creation of $LiFePO_4$–Fe_2P–C composites with a porous conductive architecture, which includes distinct regions or clusters containing antiferromagnetic (AFM) $LiFePO_4$ in close proximity to ferromagnetic (FM) Fe_2P. Most of the reported solid state reaction methods basically are a combination of high energy ball-milling, followed by a solid state reaction. Before solid state reaction, high energy ball milling process is required to mix the starting materials in an atomic level for a longer period of time, which is obviously energy and time consuming as well.

Herein, this article reports on very simple ultra-fast solvent assisted manual grinding method instead of high energy ball milling to ensure intimate and homogeneous mixing of elements at the atomic level, so that the $LiFePO_4$ particles incorporated with amorphous carbon and conductive Fe_2P phase could be formed *in situ* after being calcined in a two-step process under Ar atmosphere. This research also presents evidence consistent with the occurrence of an AFM/FM "exchange bias" (EB) effect, as evidenced by a particular type of shifting of the magnetic hysteresis loops. Based on these results and those of others, at least in part, the electrochemical performance of $LiFePO_4$–Fe_2P–C composite cathodes is enhanced by increasing the volume fraction of fine distributions of $LiFePO_4$/Fe_2P. Electrochemical measurements demonstrated that the synthesised $LiFePO_4$–Fe_2P–C composite delivered a high capacity of 167 mAh g^{-1} at 0.2 C at the 100th cycle and displayed long term cycling stability with a capacity retention of around 96% (131 mAh g^{-1}), even after 1000 cycles at 10 C. To the best of our knowledge, this is the best high rate long-term cycling performance for $LiFePO_4$/C composite cathode material reported so far.

2. Experimental

2.1. Materials synthesis

A simple ultra-fast solvent assisted manual grinding method, combined with solid state reaction, has been developed to synthesize $LiFePO_4$–Fe_2P–C composite with a porous conductive architecture. The grinding method presented here replaces the time-consuming high energy ball-milling method. Li_2CO_3, $FeC_2O_4{\cdot}2H_2O$, and $NH_4H_2PO_4$ in a stoichiometric molar ratio of 1:1:1 were used as starting materials, and citric acid ($C_6H_8O_7$) was used as a reducing agent and carbon source as well. The reactants for preparing the precursor were ground thoroughly, and a slurry was made by mortar and pestle in acetone solvent to ensure intimate and homogeneous mixing at the atomic level. The slurry was then dried in an oven at 60 °C to remove acetone from the slurry. To decompose the carbonate, oxalate, and phosphate, the dried mixture was placed in a tube furnace and heat-treated at 350 °C for 10 h under flowing argon. The resultant powders were cooled to room temperature and thoroughly reground. The powders were again calcined at 600 °C for 10 h under argon flow. Thus the bare-$LiFePO_4$ and $LiFePO_4$–Fe_2P–C composites containing 5.8 wt.% C [$LiFePO_4$–Fe_2P–C (1)], 10.4 wt.% C [$LiFePO_4$–Fe_2P–C (2)], and 19.9 wt.% C [$LiFePO_4$–Fe_2P–C (3)] were obtained using different amounts of citric acid used.

2.2. Composition and structure determination

X-ray diffraction (XRD) data were collected on a GBC MMA generator. Traces™ software in combination with the Joint Committee on Powder Diffraction Standards (JCPDS) powder diffraction files was used to identify the phases present. The Brunauer–Emmett–Teller (BET) surface areas of the synthesized materials were measured by a NOVA 1000 high speed gas sorption analyzer (Quantachrome Corporation, USA). Magnetic measurements were performed using a physical properties measurement system (PPMS) 14 T magnetometer. The amounts of amorphous carbon in the composite samples were estimated using a thermogravimetric analysis/differential scanning calorimetry (TGA/DSC) 1 Star^e System. The morphologies and microchemistries of the samples were investigated by a field emission scanning electron microscopy-energy dispersive X-ray spectroscopy (FESEM-EDS) system (JEOL JSM-7500FA with Bruker EDS analysis system) and transmission electron microscopy (TEM) (JEOL 2011, 200 kV). Samples for secondary electron imaging were prepared by dispersion onto carbon tape, while samples for high contrast backscattered imaging analysis were prepared by mounting in conducting phenolic followed by metallographic grinding and polishing for examination in sections. TEM samples were prepared by deposition of ground particles onto holey carbon support films.

2.3. Electrode preparation, coin cell assembly, and electrochemical measurements

To test the electrochemical performance, powder samples were mixed with acetylene black (AB) (Cabot Australasia Pty Ltd.) and a binder, polyvinylidene fluoride (PVdF, Sigma–Aldrich), in a weight ratio of 80:15:5 in a solvent, *N*-methyl-2-pyrrolidone (NMP, Sigma–Aldrich, anhydrous, 99.5%). The slurry was uniformly spread onto aluminium foil substrates with a loading of 1.5–2.0 mg cm^{-2}. The coated electrodes were dried in a vacuum oven at 100 °C for 24 h and then pressed. CR 2032 coin-type cells were assembled in an Ar-filled glove box (Mbraun, Unilab, Germany). The electrochemical coin cells contained the coated materials on aluminium foil as the working electrode, lithium foil as counter electrode and reference electrode, porous polypropylene as the separator, and 1 M $LiPF_6$ in a 50:50 (v/v) mixture of ethylene carbonate and dimethyl carbonate (MERCK KgaA, Germany) as the electrolyte. The cells were galvanostatically charged and discharged in the range of 4.3–2.5 V at different rates of 0.2–10 C using a computer-controlled charger system manufactured by Neware Battery Testers. Cyclic voltammetry (with a scan rate of 0.1 mV s^{-1} between 4.3 and 2.5 V (versus Li/Li^+)) and electrochemical impedance spectroscopy (EIS) were performed on the electrodes using a CHI 660C electrochemistry workstation. The AC amplitude was 5 mV, and the frequency range applied was 100 kHz to 0.01 Hz.

3. Results and discussion

X-ray diffraction (XRD) results obtained from the samples are shown in Fig. 1. The profiles of the diffraction peaks could be indexed according to the olivine $LiFePO_4$ phase (JCDPS Card Number 40-1499). Any broad peaks or lines corresponding to amorphous or crystalline carbon were of insufficient intensity to be detected against the background in the XRD pattern of the $LiFePO_4$–Fe_2P–C composites. XRD patterns obtained from the carbon coated samples indicate that iron phosphide phase (barringerite Fe_2P, peak at $2\theta = 40.28°$) begins to form during the annealing process. According to the literature, it usually exists in the form of nanosized clusters [14]. We also have collected XRD patterns from bare-$LiFePO_4$ and have not found evidence of Fe_2P

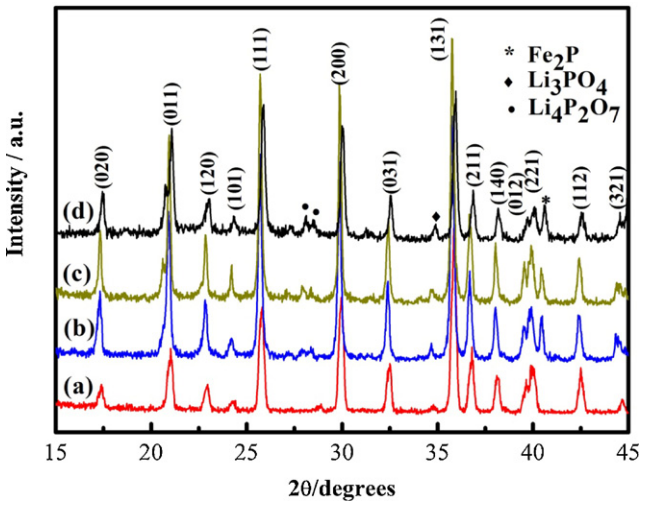

Fig. 1. XRD patterns of the samples: (a) bare-$LiFePO_4$ (0 wt.% C), (b) $LiFePO_4$–Fe_2P–C (1) (5.8 wt.% C), (c) $LiFePO_4$–Fe_2P–C (2) (10.4 wt.% C) and (d) $LiFePO_4$–Fe_2P–C (3) (19.9 wt.% C).

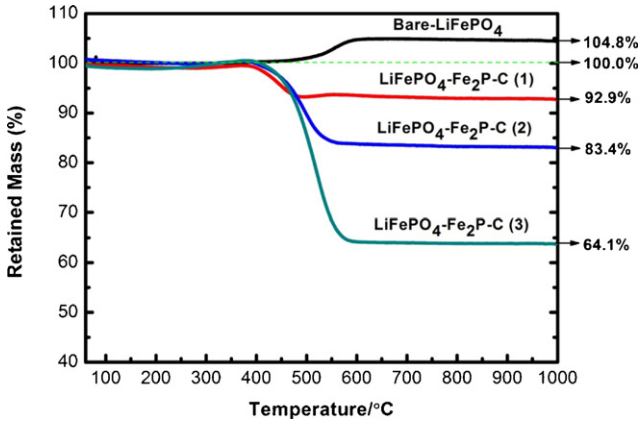

Fig. 2. TGA curves of bare-$LiFePO_4$ and $LiFePO_4$–Fe_2P–C composite powders estimated to contain (1) 5.8 wt.% C, (2) 10.4 wt.% C and (3) 19.9 wt.% C.

peaks. It is therefore possible that carbon originating from the citrate framework has acted as a reductant under the Ar atmosphere during the annealing process in our synthesis system. The generation of barringerite (Fe_2P) is the reduction of phosphate and iron in the precursor by the presence of any reductive under the inert atmosphere [15]. During the annealing process, most amorphous $LiFePO_4$ phase gradually crystallizes and aggregates, but a little nearby element Fe^{2+} and P^{5+} would have chance to be deoxidized to Fe_2P by coating carbon at the surface of $LiFePO_4$ particle and forms minor Li_3PO_4 phase at the same time [16]. To estimate the amount of amorphous carbon in the $LiFePO_4$–Fe_2P–C composites, TGA was carried out in air (Fig. 2). The samples were heated from 50 to 1000 °C at a rate of 5 °C min^{-1}. As can be seen from Fig. 2, bare-$LiFePO_4$ and $LiFePO_4$–Fe_2P–C powders started to oxidize slowly in air at temperatures above 365 °C, with rapid oxidation above 450 °C. The retained mass of the bare-$LiFePO_4$ powder was increased by 4.8 wt.%, which could be attributed to the oxidation of Fe(II) to Fe(III). Meanwhile, the $LiFePO_4$–Fe_2P–C composite powders showed rapid mass loss between 400 and 700 °C, which corresponds to the burning of carbon. The difference in weight between bare-$LiFePO_4$ and $LiFePO_4$–Fe_2P–C powders after the oxidation could be translates into the amount of amorphous carbon in the composites. With the use of this method, it was estimated that the amount of amorphous carbon in the composites were approximately 5.8 wt.% C [$LiFePO_4$–Fe_2P–C (1)], 10.4 wt.%

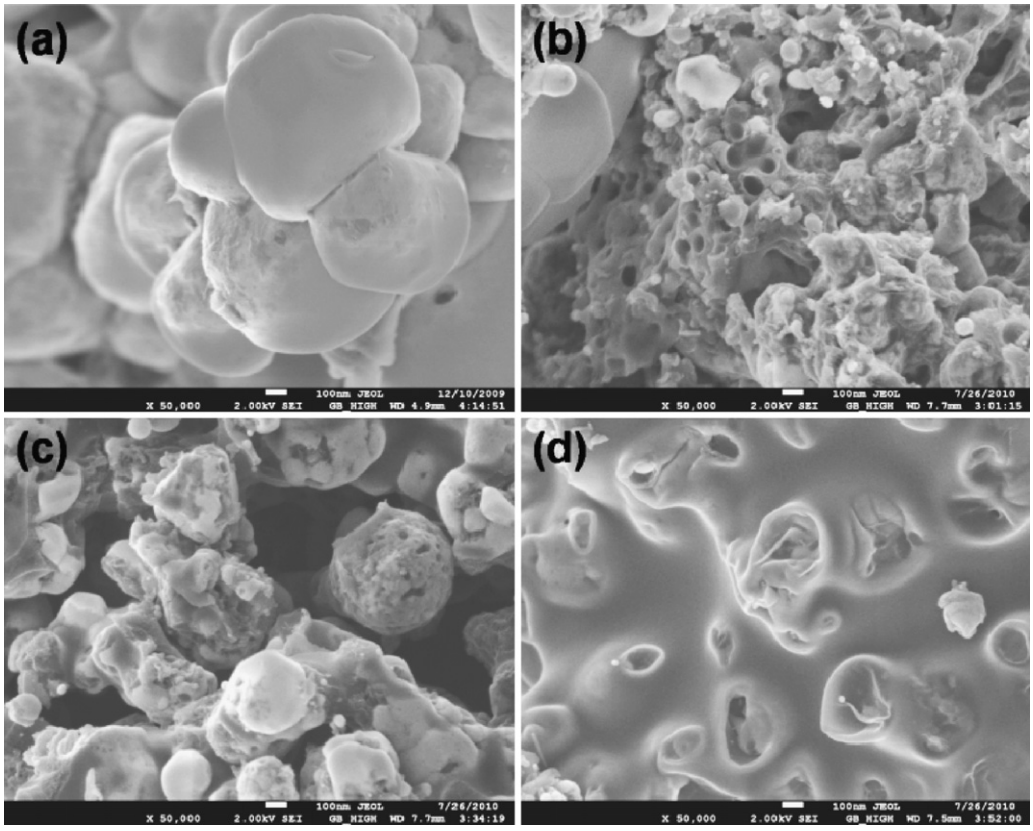

Fig. 3. Secondary electron FESEM micrographs of (a) bare-$LiFePO_4$, (b) $LiFePO_4$–Fe_2P–C (1), (c) $LiFePO_4$–Fe_2P–C (2) and (d) $LiFePO_4$–Fe_2P–C (3).

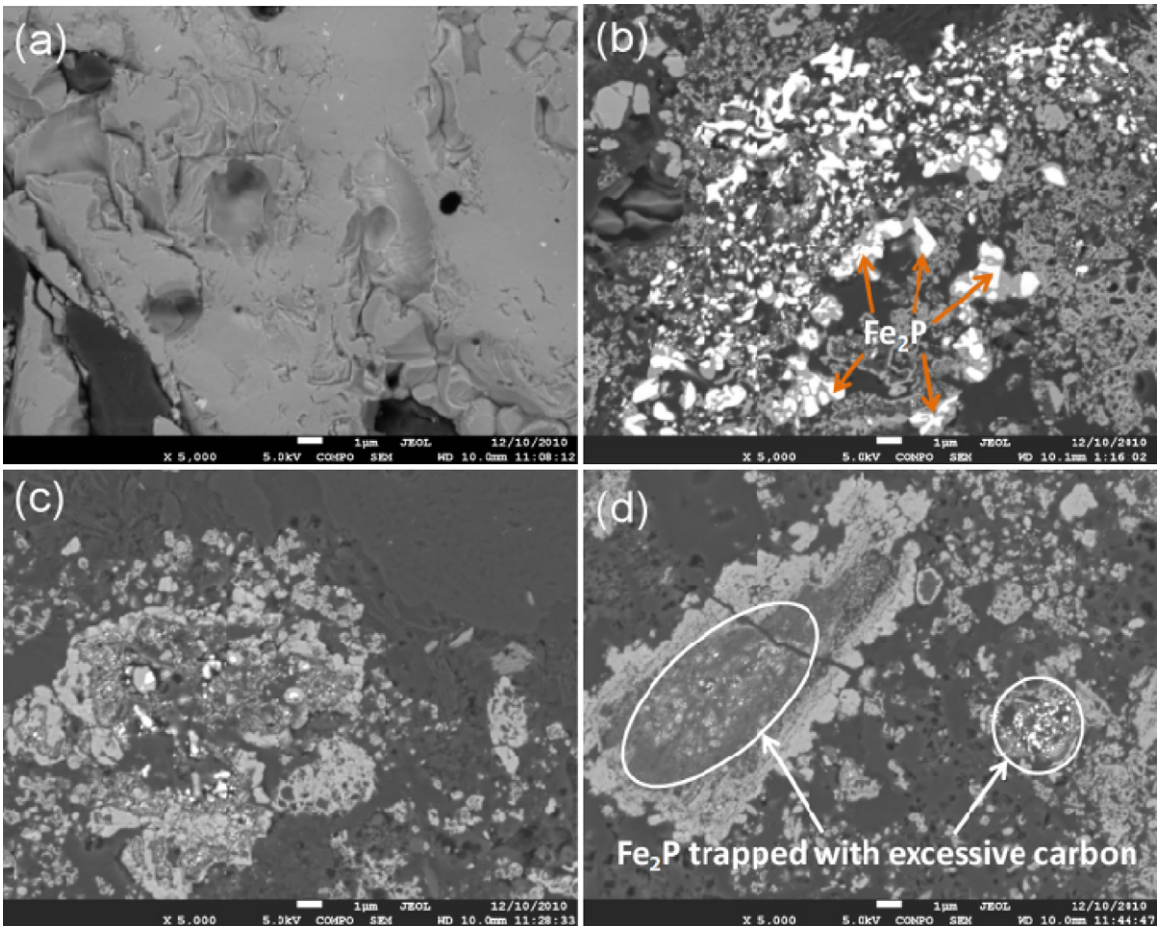

Fig. 4. High contrast backscattered FESEM micrographs of (a) bare-$LiFePO_4$, (b) $LiFePO_4$–Fe_2P–C (1), (c) $LiFePO_4$–Fe_2P–C (2) and (d) $LiFePO_4$–Fe_2P–C (3).

C [$LiFePO_4$–Fe_2P–C (2)], and 19.9 wt.% C [$LiFePO_4$–Fe_2P–C (3)], as obtained from different amounts of citric acid used. The specific surface areas of the synthesised products were also measured by the 15 points Brunauer–Emmett–Teller (BET) N_2 adsorption method. The $LiFePO_4$–Fe_2P–C (1) composite containing 5.8 wt.% C shows the highest specific surface area (33.14 $m^2\ g^{-1}$), while bare-$LiFePO_4$, $LiFePO_4$–Fe_2P–C (2) (10.4 wt.% C), and $LiFePO_4$–Fe_2P–C (3) (19.9 wt.% C) have specific surface areas of 1.17, 16.74, and 14.25 $m^2\ g^{-1}$, respectively.

Secondary electron field emission scanning electron microscopy (FESEM) images of the bare-$LiFePO_4$ and $LiFePO_4$–Fe_2P–C composites with different carbon contents are shown in Fig. 3. It was observed that the growth of the $LiFePO_4$ grains is inhibited by the carbon and Fe_2P that are formed during the heat treatment process. According to previous investigations, the particle size and electrochemical polarization can be reduced effectively when the $LiFePO_4$ particle surface is coated by conductive carbon [10,17]. In Fig. 3(b)–(d), the FESEM images indicate more abrupt particle growth with increasing carbon content in the sample, which may be caused by the agglomeration of excess carbon in the sample where Fe_2P nanoclusters are being trapped. The porous network structure, along with small particles and rough surfaces, can be clearly observed in Fig. 3(b). As shown in Fig. 3(c) and (d), it is obvious that with increasing carbon content, the porous network structure with rough surfaces gradually disappears, while agglomerated larger particles with smooth surfaces appear. FESEM high-contrast backscattered imaging (Fig. 4) of the powders was performed with qualitative calibration of the three most distinct phases (Fe_2P, $LiFePO_4$, and C) that are present in local regions of constant grey level. This was achieved by using energy dispersive spectroscopy (EDS) spot analysis performed on regions of constant grey level (Fig. 5). The light grey regions in the FESEM image are composed of $LiFePO_4$ particles with amorphous carbon (Fig. 5(a)), whereas the greyish white regions represent Fe_2P particles with amorphous carbon (Fig. 5(b)). Examination of Fig. 4(b)–(d) reveals the presence of inhomogeneous distributions of nanoscale Fe_2P particles (white), in a highly porous architecture of $LiFePO_4$ (light grey) and carbon (dark grey). Despite the inhomogeneous nature of the microstructures, it was observed that the $LiFePO_4$–Fe_2P–C composite containing 5.8 wt.% C (Fig. 4(b)) exhibited the largest fraction of local areas with a fine distribution of Fe_2P particles in close contact with $LiFePO_4$ and carbon (compare Fig. 4(b) with Fig. 4(c) and (d)). It was also observed that this sample (5.8 wt.% C) had a particularly porous conductive architecture (Supporting Information, Fig. S1). These observations are consistent with the formation of a higher fraction of $LiFePO_4$/Fe_2P interface coupling, with implications for magnetic properties. With increasing carbon content, the Fe_2P particles become connected with the primary particles of $LiFePO_4$ and also become denser. This is caused by the agglomeration of the excess carbon in the sample where Fe_2P particles are being trapped (Fig. 4(d)).

Preliminary magnetic measurements revealed additional information which can be associated with structural evolution in the samples. The exchange interaction at the interface between a ferromagnetic (FM) and antiferromagnetic (AFM) component often results in an interesting phenomenon called “exchange bias” (EB), which is manifested by a shift in the hysteresis loop along the field axis when the system is cooled down in an external magnetic

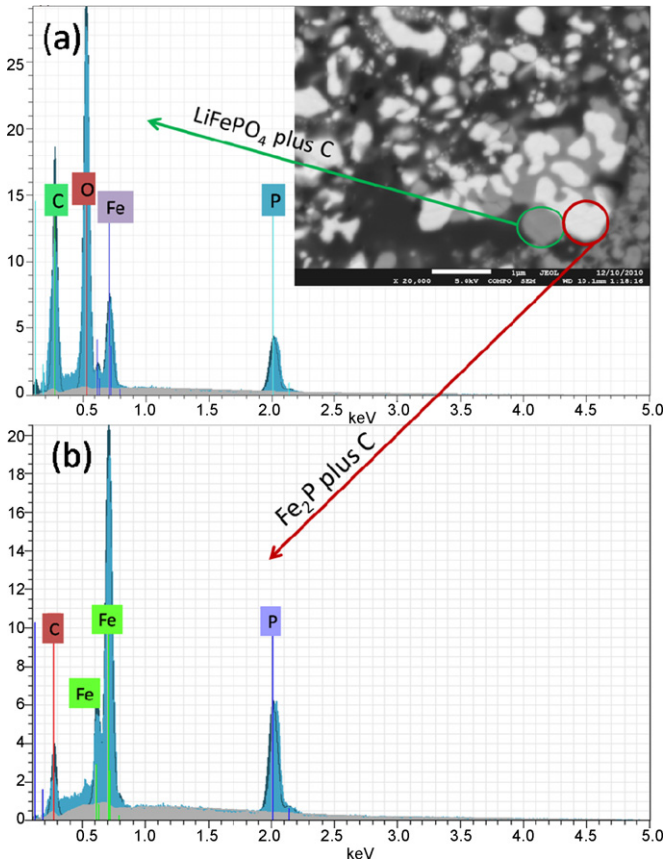

Fig. 5. EDS spectra of particles in $LiFePO_4$–Fe_2P–C composite: (a) $LiFePO_4$/C particle, with high contrast, backscattered FESEM image of source particle in the inset and (b) $Fe_2P\,C^{-1}$ particle, with arrow indicating source particle in (a) inset.

field [20,21]. So far, there has been no experimental determination of an exchange bias (EB) effect in $LiFePO_4/Fe_2P$ interface coupling in $LiFePO_4$ materials, even though the magnetic structure and properties of $LiFePO_4$ have been re-examined theoretically and experimentally [18,19]. Compared to the other samples investigated, a large shift was observed in the magnetic hysteresis loop for the sample containing 5.8 wt.% C. Assuming that this shift is associated with an exchange bias effect, the magnitude of this shift in the field axis can be defined as the EB (exchange bias) field, $-H_E = (H_1 + H_2)/2$, where H_1 and H_2 are the left and right coercive fields, respectively [20]. Results for different samples are shown in Fig. 6. The maximum value of H_E is 634 Oe with a 500 Oe cooling field for the 5.8 wt.% C containing sample, which is larger than the value for the other samples at 5 K. Comparison of the EB effect among the samples indicates that the effect is stronger for the 5.8 wt.% C containing sample and is in descending order of $LiFePO_4$–Fe_2P–C (1) > $LiFePO_4$–Fe_2P–C (2) > $LiFePO_4$–Fe_2P–C (3). This trend is coincident with the observation that the fraction of local areas containing a fine distribution of Fe_2P particles in close contact with $LiFePO_4$ also decreases in the same way, where the largest fraction is observed in the sample containing 5.8 wt.% C. The same trend was also observed for surface area measurements, with BET surface areas of 33.14, 16.74, 14.25, and 1.17 $m^2\,g^{-1}$ for the 5.8, 10.4, and 19.9 wt.% C containing samples and bare-$LiFePO_4$, respectively, and in electrochemical impedance spectroscopy (EIS) analysis (described later). Transmission electron microscopy (TEM) was used to investigate the morphology and structure of the bare sample and 5.8 wt.% C composite (Supporting Information, Figs. S2 and S3). It was clearly observed that the crystallite size of this composite is much smaller than that of the bare $LiFePO_4$ (Fig. S2). High-resolution transmission electron microscopy (HRTEM) examination also exhibits the presence of interface coupling of $LiFePO_4/Fe_2P$ clusters in the sample (Fig. S3).

The electrochemical performances of the prepared samples were evaluated systematically using CR2032 coin cells (Fig. 7). The short-term cycle life performances of the bare-$LiFePO_4$ and $LiFePO_4$–Fe_2P–C composite electrodes at 10 C charge/discharge rates are shown in Fig. 7(a). The initial discharge capacities were measured to be 43, 59, 89, and 137 mAh g^{-1} with a capacity retention of 40, 56, 84, and 136 mAh g^{-1} at the 120th cycle at the 10 C rate for the bare-$LiFePO_4$, $LiFePO_4$–Fe_2P–C (3), $LiFePO_4$–Fe_2P–C (2), and $LiFePO_4$–Fe_2P–C (1) electrodes, respectively. The electrochemical performance among the carbon coated samples is in descending order of $LiFePO_4$–Fe_2P–C (1) > $LiFePO_4$–Fe_2P–C (2) > $LiFePO_4$–Fe_2P–C (3). The electrode composed of $LiFePO_4$–Fe_2P–C (1) (5.8 wt.% C) shows the best electrochemical performance, even at the high current density of 10 C. In order to fully estimate the electrochemical performance of the $LiFePO_4$–Fe_2P–C (1) (5.8 wt.% C) composite electrode, the cycling behaviours at different current densities of 0.2, 2, 5 and 10 C were measured at the 100th cycle, and their corresponding charge–discharge voltage profiles are shown in Fig. 7(c). The $LiFePO_4$–Fe_2P–C (1) (5.8 wt.% C) composite electrode shows long and flat voltage plateaus in the 3.4–3.5 V range, and the small voltage difference between the charge–discharge plateaus indicates its good kinetics. This observation is also supported by the cyclic voltammogram (CV curve) shown in Fig. 7(d). The well defined sharp redox peaks in the range of 3.26–3.70 V can be attributed to the Fe^{2+}/Fe^{3+} redox couple reaction, corresponding to lithium extraction and insertion in the $LiFePO_4$ crystal structure [2]. The 100th cycle discharge capacities were measured to be 167 mAh g^{-1} at 0.2 C, 159 mAh g^{-1} at 2 C, 146 mAh g^{-1} at 5 C, and 136 mAh g^{-1} at 10 C for the $LiFePO_4$–Fe_2P–C (1) (5.8 wt.% C) electrode, respectively. At the low current density of 0.2 C (5 h charge and 5 h discharge), the discharge capacity (167 mAh g^{-1}) is very close to the theoretical capacity of $LiFePO_4$ (170 mAh g^{-1}). Even at the high current rate of 10 C (6 min for charging and 6 min for discharging), a capacity of 136 mAh g^{-1} is still obtained, demonstrating that the $LiFePO_4$–Fe_2P–C (1) (5.8 wt.% C) composite can tolerate high rate charge and discharge. The capacity fading observed is only ~18% with increasing of charge–discharge rate from 0.2 to 10 C. Our composite electrode was life tested at a high current density of 1700 mA g^{-1} (10 C rate) for long term cycling, as batteries are required to operate at high current density and to have a cycle life of more than 2000 cycles for EV/HEV applications [22]. Therefore, we cycled $LiFePO_4$–Fe_2P–C (1) (5.8 wt.% C) electrode at the 10 C rate (6 min for charging and 6 min for discharging) for 1000 cycles (Fig. 7(b)). Surprisingly, the $LiFePO_4$–Fe_2P–C (1) (5.8 wt.% C) electrode exhibited superior electrochemical performance, with a capacity retention of around 96% (131 mAh g^{-1}) of its original discharge capacity after 1000 cycles at the high current rate of 10 C. Such outstanding electrochemical performance certainly can meet the demands of many high power applications.

To understand the effect of $LiFePO_4/Fe_2P$ interface coupling along with that of the carbon coating on the charge transfer resistance of electrodes, ac impedance measurements were carried out at room temperature (Fig. 7(e)). The impedance curves show one compressed semicircle in the medium-frequency region, which could be assigned to the charge-transfer resistance (R_{ct}). The spike or inclined line at the low frequency end indicates the Warburg impedance (W) of long-range lithium-ion diffusion [23–25]. The charge transfer resistance (R_{ct}) was calculated to be 148 Ω cm^{-2} for the bare-$LiFePO_4$, 28 Ω cm^{-2} for the $LiFePO_4$–Fe_2P–C (1), 37 Ω cm^{-2} for the $LiFePO_4$–Fe_2P–C (2), and 60 Ω cm^{-2} for the

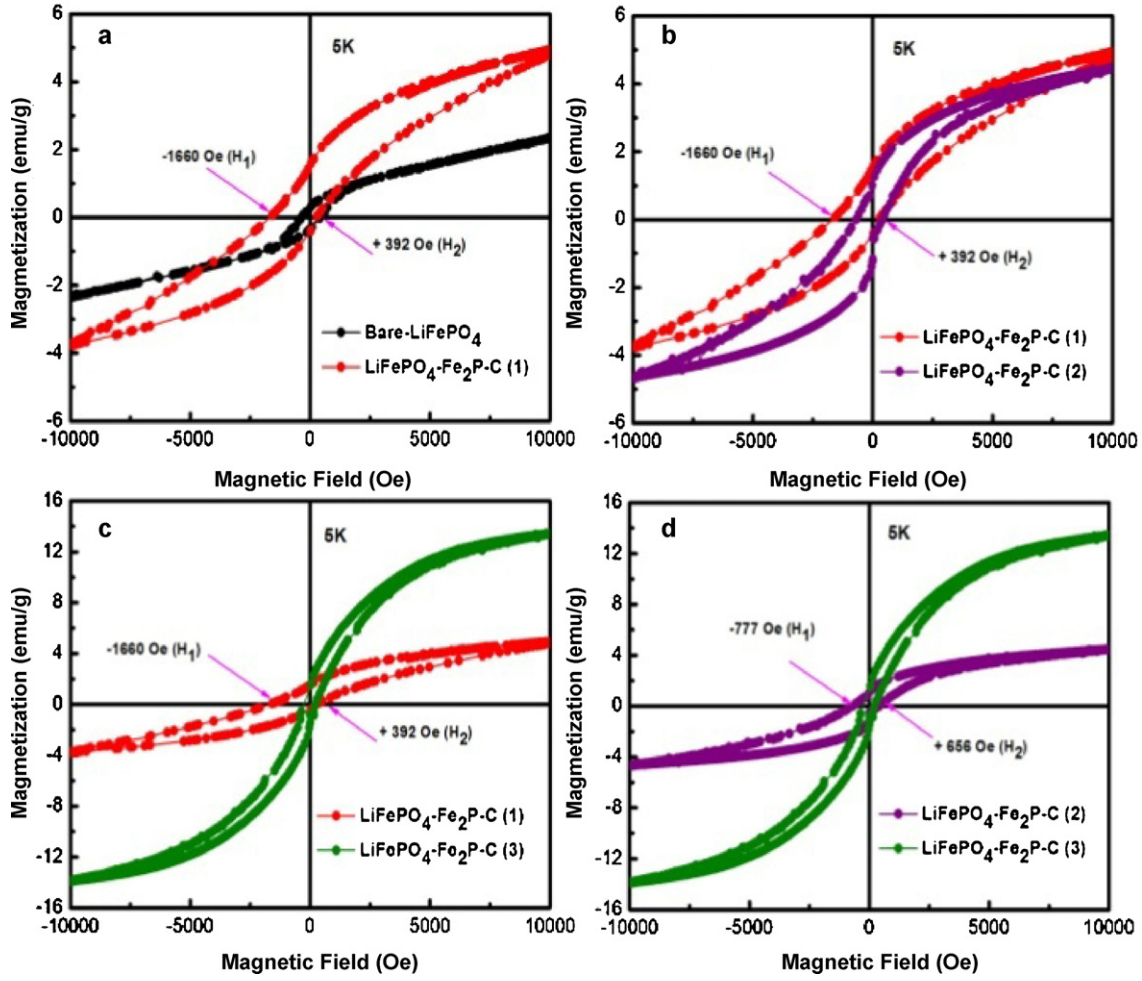

Fig. 6. Magnetic hysteresis loops measured at 5 K between ±10,000 Oe after field cooling in 500 Oe.

$LiFePO_4$–Fe_2P–C (3) electrodes, respectively. According to a previous report [26], a higher carbon content sample shows lower charge transfer resistance (R_{ct}), and generally, this trend is also logical. Under this consideration, the R_{ct} should be in order of $LiFePO_4$–Fe_2P–C (3) (19.9 wt.% C) < $LiFePO_4$–Fe_2P–C (2) (10.4 wt.% C) < $LiFePO_4$–Fe_2P–C (1) (5.8 wt.% C), but the reality is the inverse, since $LiFePO_4$–Fe_2P–C (1) < $LiFePO_4$–Fe_2P–C (2) < $LiFePO_4$–Fe_2P–C (3). At this point, we contend that this R_{ct} is not only influenced by the carbon content, but also strongly influenced by the interface coupling of $LiFePO_4$/Fe_2P clusters. The $LiFePO_4$–Fe_2P–C (1) sample exhibits more and stronger interface coupling of antiferromagnetic (AFM) and ferromagnetic (FM) clusters than the other samples, which increases the effective interface areas, facilitates more rapid charge transfer, and reduces the charge transfer resistance, leading to the huge shift in the magnetic hysteresis loop [27,28].

This enhanced kinetics, superior high rate performance, and long term cycling stability of the $LiFePO_4$–Fe_2P–C (1) (5.8 wt.% C) electrode could be explained as follows:

The parent $LiFePO_4$ materials are insulating in nature and clearly, there is a need for nanosizing and/or carbon coating of these materials to increase ionic and electronic conductivity. Attributed to its excellent electrical conductivity, superior chemical/electrochemical stability, and unique physical properties, the carbon coating layer acts as a multi-functional layer between the active $LiFePO_4$ particles and electrolyte to enhance the electrode conductivity, reduce the surface activity of particles, improve the solid electrolyte interface (SEI) film, protect the active material from electrolyte corrosion, and maintain the electrode integration and conductivity upon volume change, thus resulting in much improved rate capability and cycle stability of the coated materials [29]. Carbon coating layer also reduces side reactions between $LiFePO_4$ and electrolyte which prevents $LiFePO_4$ particles from directly contacting with electrolyte. It can also be assumed that the presence of conductive Fe_2P phase in the composite acts as important role in increasing electronic conductivity and evidently improves the electrochemical performance of $LiFePO_4$/C including the less polarization phenomenon, comparatively high reversible capability, stable cycling performance and slight trend of less loss of rate capability [16,30]. However, only a proper carbon content (here 5.8 wt.% C) can lead to a more uniform distribution of carbon and Fe_2P clusters and also help to create a porous architecture of the materials at the same time. It is believed that the carbon content maybe a critical factor for the carbon distribution around particles and the formation of $LiFePO_4$/Fe_2P interface coupling. It was observed that with the increasing carbon content, the Fe_2P particles connect with the primary particles of $LiFePO_4$ and become denser caused by the agglomeration of the excessive carbon in the sample where Fe_2P particles are being trapped, leading to a low specific surface area. So, the excellent electrochemical performances of the $LiFePO_4$–Fe_2P–C (1) (5.8 wt.% C) composite could be attributed to the porous conductive architecture of the materials with proper carbon content, huge and strong interface coupling of $LiFePO_4$/Fe_2P that increase the contact area among the carbon, Fe_2P

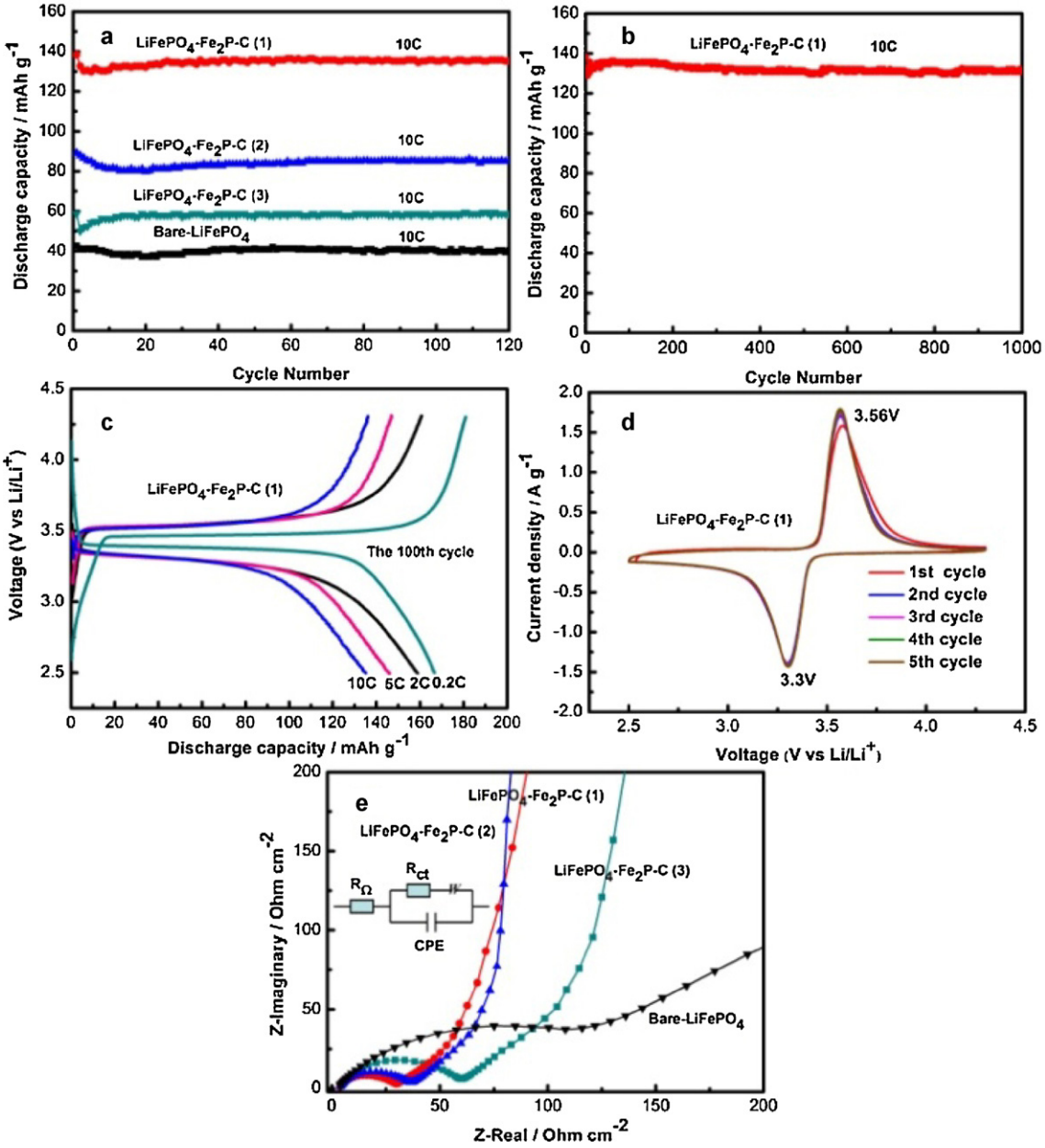

Fig. 7. Short-term cycle life performance (a), long-term cycle life performance beyond 1000 cycles at 10 C for the $LiFePO_4$–Fe_2P–C (1) electrode (b), the 100th cycle galvanostatic charge–discharge profiles at different current densities from 0.2 to 10 C between 4.3 and 2.5 V for $LiFePO_4$–Fe_2P–C (1) electrode (c), cyclic voltammogram of $LiFePO_4$–Fe_2P–C (1) electrode at a scan rate of 0.1 mV s^{-1} (d) and EIS spectra of the bare-$LiFePO_4$ and $LiFePO_4$–Fe_2P–C electrodes, and the equivalent circuit (inset) (e).

clusters, and $LiFePO_4$ particles, providing multi-dimension channels for charge transfer and reduce the resistances for lithium ion migration. Moreover, the composite with porous architecture can suck up electrolyte to shorten enormously the diffusive distance of lithium ion.

4. Conclusions

In conclusion, the results have demonstrated that the fabrication of samples with strong and extensive antiferromagnetic (AFM) and ferromagnetic (FM) interface coupling of $LiFePO_4/Fe_2P$ provides a versatile strategy toward improving the electrochemical properties of $LiFePO_4$ materials and also opens up a new window for material scientists to further study the new exchange bias phenomenon and its ability to enhance the electrochemical performance of lithium-ion battery electrode.

Acknowledgements

The authors are grateful for funding from the Australian Research Council (ARC) under an ARC Centre of Excellence Program (CE0561616) and an ARC Discovery project (DP0987805). The authors also thank Dr. T. Silver for critical reading of the manuscript.

Appendix A. Supplementary data

Supplementary data associated with this article can be found, in the online version, at doi:10.1016/j.jpowsour.2012.01.119.

References

[1] D. Liu, G. Cao, Energy Environ. Sci. 3 (2010) 1218–1237.
[2] G. Wang, H. Liu, J. Liu, S. Qiao, G.M. Lu, P. Munro, H. Ahn, Adv. Mater. 22 (2010) 4944–4948.

[3] M.M. Rahman, J.Z. Wang, M.Z. Hassan, S. Chou, Z. Chen, H.K. Liu, Energy Environ. Sci. 4 (2011) 952–957.
[4] B. Scrosati, J. Garche, J. Power Sources 195 (2010) 2419–2430.
[5] T. Zhang, L.J. Fu, H. Takeuchi, J. Suzuki, K. Sekine, T. Takamura, Y.P. Wu, J. Power Sources 159 (2006) 349–352.
[6] T. Zhang, L.J. Fu, J. Gao, L.C. Yang, Y.P. Wu, H.Q. Wu, Pure Appl. Chem. 78 (2006) 1889–1896.
[7] M.J. Noh, Y. Kwon, H. Lee, J. Cho, Y. Kim, M. Kim, Chem. Mater. 17 (2005) 1926–1929.
[8] A.K. Padhi, K.S. Nanjundaswamy, J.B. Goodenough, J. Electrochem. Soc. 144 (1997) 1188–1194.
[9] A. Yamada, S.C. Chung, K. Hinokuma, J. Electrochem. Soc. 148 (2001) A224–A229.
[10] H. Huang, S.C. Yin, L.F. Nazar, Electrochem. Solid State Lett. 4 (2001) A170–A172.
[11] Z.H. Chen, J.R. Dahn, J. Electrochem. Soc. 149 (2002) A1184–A1189.
[12] B. Kang, G. Ceder, Nature 458 (2009) 190–193.
[13] S.J. Kwon, C.W. Kim, W.T. Jeong, K.S. Lee, J. Power Sources 137 (2004) 93–99.
[14] A.A. Salah, A. Mauger, C.M. Julien, F. Gendron, Mater. Sci. Eng. B 129 (2006) 232–244.
[15] G. Arnold, J. Garche, R. Hemmer, S. Strobele, C. Vogler, M. Wohlfahrt-Mehrens, J. Power Sources 119–121 (2003) 247–251.
[16] Y. Xu, Y. Lu, L. Yan, Z. Yang, R. Yang, J. Power Sources 160 (2006) 570–576.
[17] Y. Wang, Y. Wang, E. Hosono, K. Wang, H. Zhou, Angew. Chem. Int. Ed. 47 (2008) 7461–7465.
[18] V.A. Streltsov, E.L. Belokoneva, V.G. Tsirelson, N.K. Hansen, Acta Crystallogr. B 49 (1993) 147–153.
[19] G. Rousse, J.R. Carvajal, S. Patoux, C. Masquelier, Chem. Mater. 15 (2003) 4082–4090.
[20] W.H. Meiklejohn, C.P. Bean, Phys. Rev. 102 (1956) 1413–1414.
[21] J. Nogués, J. Sort, V. Langlais, V. Skumryev, S. Suriñach, J.S. Muñoz, M.D. Baró, Phys. Rep. 422 (2005) 65–117.
[22] J. Liu, J. Wang, X. Yan, X. Zhang, G. Yang, A.F. Jalbout, R. Wang, Electrochim. Acta 54 (2009) 5656–5659.
[23] F. Gao, Z. Tang, Electrochim. Acta 53 (2008) 5071–5075.
[24] H.C. Shin, W.I. Cho, H. Jang, J. Power Sources 159 (2006) 1383–1388.
[25] H.H. Chang, C.C. Chang, C.Y. Su, H.C. Wu, M.H. Yang, N.L. Wu, J. Power Sources 185 (2008) 466–472.
[26] X. Zhi, G. Liang, L. Wang, X. Ou, L. Gao, X. Jie, J. Alloys Compd. 503 (2010) 370–374.
[27] K. De, M. Patra, S. Majumdar, S. Giri, J. Phys. D: Appl. Phys. 41 (2008) 175007.
[28] L. Liu, S.L. Yuan, Z.M. Tian, X. Liu, J.H. He, P. Li, C.H. Wang, X.F. Zheng, S.Y. Yin, J. Phys. D: Appl. Phys. 42 (2009) 045003.
[29] H. Li, H. Zhou, Chem. Commun. 48 (2012) 1201–1217.
[30] P.S. Herle, B. Ellis, N. Coombs, L.F. Nazar, Nat. Mater. 3 (2004) 147–152.